InSAR constrains on coseismic and postseismic deformation of the 2021 Ganaveh earthquake along the Zagros foredeep fault

Institute for Advanced Studies in Basic Sciences
Gava Zang, Zanjan, Iran

ISTerre

Mahin Jafari[1], Mahtab Aflaki[1], Zahra Mousavi[1,*], Andrea Walpersdorf[2], Khalil Motaghi[1]

1. Department of Earth Sciences, Institute for Advanced Studies in Basic Sciences (IASBS), Zanjan 45137-66137, Iran , z.mousavi@iasbs.ac.ir 2. Univ. Grenoble Alpes, Univ. Savoie Mont Blanc, CNRS, IRD, Univ. Gustave Eiffel, ISTerre, 38000 Grenoble, France

Introduction

The Zagros Simply Folded belt (ZSFB) figures among the most seismically active fold and thrust belts in the world. In the central part of the ZSFB, known as the Dezful embayment (DZE) (Fig. 1), Mb > 5 earthquakes are geographically limited to the east of the Zagros foredeep fault (ZFF). The moderate magnitude (Mw 5.8) Ganaveh mainshock occurred on 2021 April 18 in the southwest part of the Dezful embayment. The reported USGS epicenter of the Ganaveh mainshock is situated in the hanging wall of the Zagros foredeep fault (ZFF) at a depth of 8 km. We take the opportunity of the accumulation of seismicity in the Dezful embayment related to the Ganaveh earthquake and its aftershocks to reanalyze the role of the ZFF as a structural borderline.

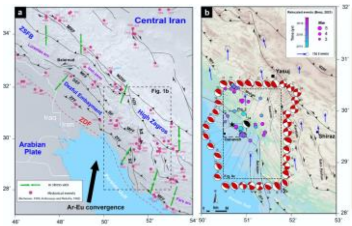

Studying the earthquake source parameters of the moderate magnitude Ganaveh event considering its location (1) in the vicinity of the structural borderline of the Mb > 5 events, and (2) in an area with a lack of relocated earthquakes, rises an opportunity to shed light on the seismic structure of the southeast part of the DZE.

Figure 1. (a) Major structure of Dezful embayment in the central part of the Zagros Simply Folded belt. The σ1 stress axes are from Authemayou et al. (2006); Lacombe et al. (2006), and Navabpour et al. (2008). (b) Active faults and earthquake focal mechanisms of the southeast part of the Dezful embayment. Focal mechanisms (Mw > 5) are from 1968 to 2018 (Nissen et al., 2011 and 2019) and from 2018 to 2022 (GCMT). The black focal mechanism shows the Ganaveh mainshock from the USGS catalog. GPS horizontal velocity field (blue vectors) is from Khorrami et al. (2019) and the Ar-EU convergence vector is from Vernant et al. (2004). Abbreviations for faults are BF: Behbahan, BZ: Borazjan, DEF: Dezful Embayment, HZF: High Zagros, Kz: Kazerun, MFF: Mountain Frontal, MRF: Main Recent, MZRF: Main Zagros Reverse, ZDF: Zagros Deformation, and ZFF: Zagros Frontal. ZSFB is Zagros Simply Folded belt.

Coseismic InSAR displacement

✓ We used the GMTSAR software (Sandwell et al., 2016) to generate interferograms from the S1-TOPS C-band SAR imagery in ascending (A101) and descending (D35) geometries.

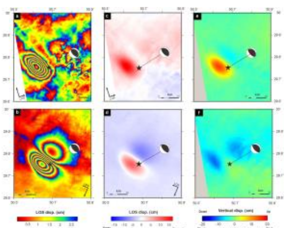

✓ The observed significant uplift and minor subsidence demonstrate a major reverse kinematic for the Ganaveh mainshock.
✓ The coseismic interferograms reveal a maximum of 17 and 15 cm displacement in the LOS direction for ascending and descending geometries, respectively.
✓ The vertical displacement map presents two lobes with significant uplift (~16 cm for the left lobe) and minor subsidence (~5 cm for the right lobe).
✓ The horizontal displacement map shows a maximum of ~11 cm westward displacement for both lobes.

Figure 2. The coseismic LOS displacement maps for the Ganaveh earthquake. The wrapped and unwrapped interferograms were acquired along ascending (a, c) and descending (b, d) orbits, respectively. The coseismic displacement maps are decomposed into vertical (e) and horizontal (f) components. The epicenter (back star) and focal mechanism solution are from USGS.

Coseismic slip modeling

✓ To obtain the source parameters, we inverted the unwrapped interferograms to infer the geometry of a single rectangular plane with uniform slip in an elastic half-space (Okada, 1985).
✓ For distributed slip modeling, we fixed the fault geometry retrieved from the uniform slip modeling, while the slip was allowed to vary freely through the plane.

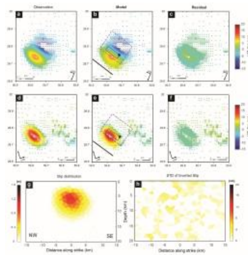

Uniform slip modeling

✓ We used the open-source software called Geodetic Bayesian Inversion Software to apply a non-linear inversion for the fault geometry (Bagnardi and Hooper, 2018).

✓ Our results indicate that the optimal model illustrates a NW-striking reverse fault plane dipping ~23° toward the northeast. The optimal fault plane is characterized by a 9.2 km length and 4.5 km width, with a uniform dip-slip of about 1.2 m.

Distributed slip modeling

✓ We used a modified version of the open-source Fault Resampler package (Barnhart and Lohman, 2010) to apply a linear inversion for calculating the slip distribution on the fault plane.

✓ Distributed slip modeling reveals that the coseismic rupture concentrates at a depth of ~6 km with a maximum slip of 95 cm along the NE-dipping reverse fault plane.

Figure 3. Observations (a and d), modeled (b and e), and residual (c and f) maps for ascending and descending geometries. Slip distribution was obtained from a linear inversion with variable slip (g) and related standard deviation (h). The solid and dashed rectangles are the modeled fault planes in the uniform and distributed slip inversion, respectively. The black solid line is the predicted surface fault trace from InSAR inversion. The black star presents the epicenter from USGS.

Applying a listric fault geometry

✓ Regarding the location of the mainshock, the concentration of the aftershocks, and the related coseismic InSAR displacements on the northeast side of the ZFF surface trace, we could suggest the Zagros foredeep fault as the causative source of the Ganaveh mainshock.
✓ Based on (1) the location of the USGS and Benz (2021) epicenters at ~6 km distance from the surface trace of the ZFF, (2) the depth of ~6 km for the maximum slip obtained from InSAR data, and (3) supposing a flat fault geometry, a ~45° dip fault plane is achieved. This is not compatible with our InSAR modeling that indicates a ~23° dip for the causative fault plane reaching the ground surface several kilometers to the southwest of the ZFF surface trace. However, by assuming a listric fault geometry for the causative fault plane, its surface trace will be compatible with the ZFF.

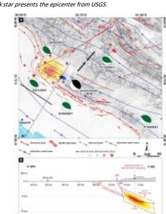

Figure 4. a) The coseismic slip distribution is superimposed on the structural map of the Ganaveh area. b) The schematic profile along the A-A' line reveals the proposed geometry of the Ganaveh causative fault.

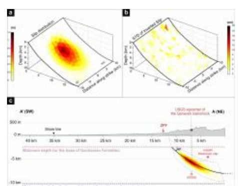

We constructed the listric fault geometry for the Ganaveh fault plane using available geological documents:

✓ upward and downward limitation to the depth of ~2 – 2.5 and 10 km as the minimum depth for the base of the Gachsaran formation and the Hormoz formation.

✓ Our InSAR modeling presents a 23° dip angle for the location of the Ganaveh slip patch. This angle decreases to zero at a depth of ~10 km and reaches a maximum of 40°-50° at shallower depths .

Figure 5. Modeled slip distribution on the listric fault plane (a) and its related standard deviation (b). c) The schematic profile along the A-A' line (Fig. 12a) shows the proposed listric geometry of the Ganaveh causative fault plane as part of the ZFF.

Postseismic deformation

To examine the postseismic displacement, we processed Sentinel 1A images by NSBAS chain (Doin et al., 2011).

The afterslip mechanism can be the causative mechanism:

(1) postseismic motion having a similar wavelength and the same direction of motion as coseismic displacement,

(2) good compatibility between the cumulative displacement, the cumulative number of aftershocks, and their related moment release through time.

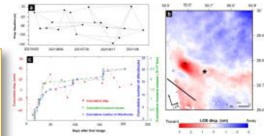

Figure 6. (a) Connection graph of images in SBAS processing. (b) The postseismic LOS cumulative displacement map. The star and the black lines present the location of the mainshock (USGS) and the predicted surface trace of the coseismic causative fault retrieved from InSAR inversion, respectively. c) The displacement through time for pixel N, compared to moment release and number of aftershocks.

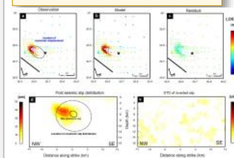

To examine the possibility of an afterslip mechanism, we inverted the cumulative postseismic displacement map to estimate the slip distribution along the causative fault plane.

The slip distribution of the postseismic motion presents a maximum of 30 cm of the dip-slip component at a depth of ~5 km slightly shallower than the coseismic slip patch.

Figure 5d indicates that the postseismic slip distribution happened in the asperity of the coseismic slip and is likely to have contributed to the stress concentration on the edge of the coseismic rupture patch.

Figure 7. Observations (a), models (b), and residual (c) maps were constructed from the distributed slip inversion for ascending data covering the postseismic phase. The blue dashed ellipsoid presents the location of the surface coseismic displacement. The star presents the epicenter from USGS. (d) Slip distribution was obtained from a linear inversion with variable slip. The black dashed and solid ellipsoids show the location of the coseismic slip patch and its maximum on the causative fault plane.

After slip relaxation time

✓ The estimated short-term deformation for the postseismic phase of the Ganaveh earthquake is released seismically by aftershocks similar to the 2010 Rigan postseismic deformation. However, the postseismic deformations for the rest of reported events in Iran were mostly released aseismically during some years.
✓ 52% and 43% of the events have a relaxation time of less than one year and between one to 10 years, respectively. Only 5% of the earthquakes were followed by long-term postseismic deformation.
✓ The geodetic postseismic to coseismic moment release ratio (Mp/Mc) for the Ganaveh earthquake is 18% and it lies within the empirically defined pattern of Mc = 10 Mp of the postseismic deformation.
✓ The coseismic interferogram time coverage and/or the locked asperities around the coseismic slip may explain the lower ratio of the Mp/Mc of the Ganaveh mainshock.

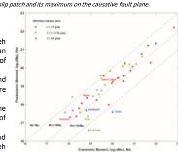

Figure 8. Mp/Mc ratio of the earthquakes occurred in Iran and around the world based on the release time.

Conclusion

✓ The Ganaveh earthquake occurred in the southeastern part of the Dezful embayment, where the modern deformation is absorbed by both thick- and thin-skin deformation along the major faults.
✓ The consequent occurrences of the coseismic rupture at the NW side of the mainshock epicenter and the postseismic rupture at the NW of the coseismic rupture asperity document the northwest propagation of the earthquake rupture. This highlights that the large magnitude aftershocks could affect the damaged buildings at the termination of the coseismic rupture and underlines the importance of the investigation of the coseismic rupture for seismic hazard assessment.
✓ Our geodetic suggest a listric geometry for the ZFF as a thin-skin thrust fault. The shallow depth of this earthquake highlights the hypothesis that in the Zagros Simply Folded Belt, the Mw < 6.1 earthquakes occurred within the sedimentary cover.

References

Authemayou, C., Chardon, D., Bellier, O., Malekzadeh, Z., Shabanian, E. and Abbassi, M.R., 2006. Late Cenozoic partitioning of oblique plate convergence in the Zagros fold-and-thrust belt (Iran). Tectonics, 25(3).
Doin, M.P., Guillaso, S., Jolivet, R., Lasserre, C., Lodge, F., Ducret, G. and Grandin, R., 2011, September. Presentation of the small baseline NSBAS processing chain on a case example: The Etna deformation monitoring from 2003 to 2010 using Envisat data. In Proceedings of the Fringe symposium (pp. 3434-3437). Frascati, Italy: ESA SP-697.
Khorrami, F., Vernant, P., Masson, F., Nilfouroushan, F., Mousavi, Z., Nankali, H., Saadat, S.A., Walpersdorf, A., Hosseini, S., Tavakoli, P. and Aghamohammadi, A., 2019. An up-to-date crustal deformation map of Iran using integrated campaign-mode and permanent GPS velocities. Geophysical Journal International, 217(2), pp.832-843.
Lacombe, O., Mouthereau, F., Kargar, S. and Meyer, B., 2006. Late Cenozoic and modern stress fields in the western Fars (Iran): implications for the tectonic and kinematic evolution of central Zagros. Tectonics, 25(1).
Navabpour, P., Angelier, J. and Barrier, E., 2008. Stress state reconstruction of oblique collision and evolution of deformation partitioning in W-Zagros (Iran, Kermanshah). Geophysical Journal International, 175(2), pp.755-782.
Nissen, E., Tatar, M., Jackson, J.A. and Allen, M.B., 2011. New views on earthquake faulting in the Zagros fold-and-thrust belt of Iran. Geophysical Journal International, 186(3), pp.928-944.
Nissen, E., Ghods, A., Karasözen, E., Elliott, J.R., Barnhart, W.D., Bergman, E.A., Hayes, G.P., Jamal-Reyhani, M., Nemati, M., Tan, F. and Abdulnaby, W., 2019. The 12 November 2017 M w 7.3 Ezgeleh-Sarpolzahab (Iran) earthquake and active tectonics of the Lurestan Arc. Journal of Geophysical Research: Solid Earth, 124(2), pp.2124-2152.
Sandwell, D., Mellors, R., Tong, X., Xu, X., Wei, M. &Wessel, P., 2016. GMTSAR: An InSAR Processing System Based on Generic Mapping Tools (2nd ed.). Technical Report.Scripps Institution of Oceanography, UC San Diego.
Vernant, P., Nilforoushan, F., Hatzfeld, D., Abbassi, M.R., Vigny, C., Masson, F., Nankali, H., Martinod, J., Ashtiani, A., Bayer, R. and Tavakoli, F., 2004. Present-day crustal deformation and plate kinematics in the Middle East constrained by GPS measurements in Iran and northern Oman. Geophysical Journal International, 157(1), pp.381-398.